Power-Law Scaling between Planck Emission and Water-Vapor Optical Depth in Radiative–Convective Equilibrium

Yi Zhang[a]

[a] *Courant Institute, New York University, New York, New York*

ABSTRACT: Water vapor is a major greenhouse gas in the Earth's atmosphere and its concentration is largely controlled by temperature according to the Clausius-Clapeyron relation. We show that, for water vapor, the Planck function and optical depth are approximately related by a power law and the exponent γ is given by the ratio of the energy of a terrestrial infrared photon ($h\nu$) to the latent heat release associated with the condensation of a single water–vapor molecule (l_v), i.e., $\gamma = h\nu/l_v$. This power law originates from the Boltzmann factor appearing in both the Clausius-Clapeyron relation and Planck's function. The power law enables analytic solutions of the Schwarzschild equation for upward and downward longwave fluxes, from which atmospheric cooling and outgoing longwave radiation (OLR) follow directly as functions of surface Planck emission and column-integrated optical depth. The nondimensional parameter γ encapsulates the dual role of water vapor as both a condensable and a greenhouse gas, and the same power law potentially applies to radiative-convective equilibrium in other planetary atmospheres.

1. Introduction

Water vapor plays two roles in the atmosphere of the Earth (Pierrehumbert 2010, e.g.). First, it is a condensable gas. With the oceans providing abundant surface reservoir, the concentration of water vapor is strongly limited by the capacity of the air to hold water vapor. This capacity is determined by the Clausius-Clapeyron relation between the saturation vapor pressure and temperature. Second, water vapor is a greenhouse gas. The bent structure of the H_2O molecule gives rise to an electric dipole moment. Molecular rotation and vibration can change the orientation and magnitude of this dipole, allowing interaction with the electromagnetic field. Transitions between rotational and rotation-vibrational states are accompanied by the absorption and emission of infrared photons, which coincide with the spectral range where much of Earth's thermal (Planck) emission is concentrated.

These two roles of water vapor are coupled through the energy budget of the atmosphere. Earth's surface absorbs incoming solar radiation far more efficiently than the atmosphere above and, as a result, the surface is systematically warmer than the overlying air. This temperature discontinuity drives vigorous vertical mixing, preventing the troposphere from attaining radiative equilibrium (Manabe and Wetherald 1967). The troposphere thus persistently loses energy through infrared radiation (e.g. Trenberth et al. 2009) and this radiative cooling is dominated by water vapor (e.g. Fig. 4.29 in Wallace and Hobbs (2006)). Cooling of the tropospheric water vapor over the broad clear-sky regions is primarily balanced by condensation heating of water vapor in the convective updrafts that occupies a tiny fraction of area, resulting in the radiative-convective equilibrium (RCE) (Manabe and Wetherald 1967),

This work concerns the radiative transfer of water-vapor-dominated wavenumbers in an RCE. A main goal is to seek an analytic expression between the Planck emission $B_{\tilde{\nu}}(T)$ and the optical depth τ in the RCE. The motivation is that the Schwarzschild's equation for radiative transfer can be expressed in the optical depth space as follows

$$\mathrm{d}I_{\tilde{\nu}} = \Big(\pi B_{\tilde{\nu}}(T) - I_{\tilde{\nu}}\Big)\mathrm{d}\tau, \tag{1}$$

where $I_{\tilde{\nu}}$ is the spectral radiation flux of wavenumber $\tilde{\nu}$ with the unit W m^{-2} cm. $I_{\tilde{\nu}}$ is intensified by the emission from the medium itself (first term on RHS) and attenuated by the medium (second term RHS) of an incremental optical depth $\mathrm{d}\tau$. The equation would be solvable if $B_{\tilde{\nu}}(T)$ can be expressed in τ. Thus, obtaining an explicit mapping between the Planck function and optical depth enables analytic solutions for radiative fluxes, and net atmospheric longwave cooling and outgoing longwave radiation would follow suit.

Seeking a relationship between $B_{\tilde{\nu}}$ and τ is not entirely straightforward because Planck emission (at a given $\tilde{\nu}$) only depends explicitly on temperature. Previous approaches have therefore proceeded in three steps: first simplifying the relationship between $B_{\tilde{\nu}}$ and temperature T, then relating temperature T to pressure p, and lastly relating p to τ.

The first step is usually done by using the grey gas model, that is integrating over the spectrum and use the T^4 relation from Stefan-Boltzmann law (Pierrehumbert 2010; Robinson and Catling 2012, e.g.) or approximating the Planck law as a power law of T (Jeevanjee and Fueglistaler 2020a). The second step corresponds to specifying the temperature

Corresponding author: Yi Zhang, y.zhang@nyu.edu

profile in pressure coordinates, which is adiabatic in radiative–convective equilibrium (RCE). For a dry adiabatic troposphere, the lapse rate is constant, implying a power-law relationship between T and p. In contrast, a moist adiabatic troposphere does not admit a closed-form $T(p)$ relation. Approximations are therefore often introduced to retain analytical tractability, typically by representing the moist adiabat with an effective constant lapse rate that is weaker than the dry one (Robinson and Catling 2012; Jeevanjee and Fueglistaler 2020a). The third step is most convenient for well-mixed gases such as CO2, for which the vertically integrated path is proportional to pressure, and pressure broadening introduces an additional factor of p, yielding $\tau_{CO_2} \propto p^2$ (Pierrehumbert 2010; Jeevanjee et al. 2021b). For condensable gases, however, the relationship is less straightforward, because the integrated path does not explicitly depend on pressure. Previous work typically assumes a scaling of the form $\tau \propto p^n$, with n often taken empirically to be a larger number such as 4 for water vapor (Frierson et al. 2006).

The various approaches described above relate $B_{\tilde{\nu}}$ to τ through coordinate transformations and involve approximations of some level of empiricism. Here, we seek a more direct mapping from $B_{\tilde{\nu}}$ to τ for water vapor. To do so, we draw on prior work formulating the atmospheric vertical structure in the temperature coordinate. Because water vapor acts both as a condensable and a greenhouse gas, expressing the atmosphere in terms of temperature reveals structural simplicity that is less apparent in traditional vertical coordinates such as height or pressure (Ingram 2010; Romps 2014; Jeevanjee 2022; Williams and Jeevanjee 2025).

Thermodynamics of dry air and water vapor determine that the temperature lapse rate and relative humidity (Romps 2014) are largely determined by temperature. Specific humidity is given by the product of relative humidity and saturation specific humidity, and is therefore primarily temperature-controlled. Moreover, the optical thickness from the top of the atmosphere to a given level is approximately proportional to the vertically integrated water vapor path (with modest modifications from pressure broadening), implying that optical depth is likewise largely a function of temperature. Since the Planck function at fixed wavenumber also depends only on temperature, radiative fluxes become, to leading order, functions of temperature alone (Ingram 2010; Jeevanjee and Romps 2018).

As a result, increases in surface temperature to leading order extend these relationships to higher temperatures near the surface, without changing the flux profile in the temperature coordinate. This leads to the near-invariance of outgoing longwave radiation with surface warming in optically thick regimes, often referred to as Simpson's law (Simpson 1928; Ingram 2010; Jeevanjee et al. 2021a). A related consequence is the fixed-anvil-temperature (FAT) hypothesis (Hartmann and Larson 2002), which links the invariant temperature level at which water vapor can no longer cool efficiently to the detrainment level of anvil clouds.

Drawing on prior work on temperature invariance in water vapor thermodynamics and radiative transfer, we argue that at a water-vapor–dominated wavenumber, both Planck emission and optical depth share a Boltzmann-like temperature dependence, $\exp(-E/k_BT)$. This implies a simple power-law relationship between the Planck function and optical depth, with an exponent determined by physical constants and the wavenumber. We then explore the applications of this power law.

The paper is organized as follows. Section 2 documents the line-by-line model for testing the theory. Section 3 and 4 are on the $B_{\tilde{\nu}} - \tau$ power law and the solutions to the Scharwartzchild equation. Section 5 and 6 are on a spectral theory for column-integrated atmospheric cooling and OLR. Section 7 evaluates the cooling-to-space approximation and discusses its accuracy in the context of the power law. Conclusions and future directions are summarized in Section 8.

2. Line-by-line radiation model and experimental setup

We use the PyRADS radiative transfer model (Koll and Cronin 2018), which incorporates the HITRAN 2016 spectroscopic database (Gordon et al. 2022) and the AER MTCKD continuum model (Mlawer et al. 2012). PyRADS provides spectrally resolved longwave radiative transfer calculations for prescribed temperature and humidity profiles and is well suited for idealized theoretical experiments.

We adopt an idealized case of the atmospheric column that exists as a choice in PyRADS. The surface radiates as a blackbody at its temperature T_s and the lowest atmospheric level has a temperature equal to T_s. For the atmospheric thermodynamic structure, we prescribe either a dry adiabatic or a moist adiabatic lapse rate extending upward from the surface temperature T_s until the temperature reaches 150 K. Above this level, the atmosphere is assumed to be isothermal, representing an idealized stratosphere with a fixed temperature (Hartmann and Larson 2002; Seeley et al. 2019). Water vapor is set to zero in the stratosphere for the purposes of this study, as the amount of water vapor in the stratosphere is usually negligible compared to that of the troposphere. Within the troposphere, relative humidity is set to be vertically uniform, with values of 30% or 70%. Surface temperature is varied from 255 to 320 K in 1 K increments. This idealized setup, namely adiabatic temperature profiles with invariant relative humidity with warming, is chosen because it represents the simplest model of the atmosphere (Manabe and Wetherald 1967).

All calculations are performed at a spectral resolution of $0.01\,\mathrm{cm}^{-1}$. The vertical grid consists of 120 pressure levels evenly spaced in linear pressure. Sensitivity tests

using up to 240 levels and linear pressure spacing or logarithmic pressure spacing produce negligible differences in the results.

3. The Planck optical-depth power law

a. Derivation

We present the theoretical grounds for the expectation that, at wavenumbers dominated by water vapor absorption, the Planck function ($B_{\tilde{\nu}}$) varies with optical depth (τ) approximately as a power law, with a constant exponent at each wavenumber $\tilde{\nu}$. First, the optical depth scales with temperature approximately following the Clausius–Clapeyron relation. Eq. (2) in the Supporting Information of Koll and Cronin (2018) provides an approximation to the water vapor path in the limit when water vapor makes a negligible contribution to atmospheric pressure and a dry adiabatic lapse rate, which states that the water vapor path $W = \int \rho q \, \mathrm{d}z$ integrated from the tropopause (stratospheric water negligible) to a certain level within the troposphere scales with $Te^*(T)$, where $e^*(T)$ is the Clausius–Clapeyron relation. Eq. (11) in Jeevanjee and Fueglistaler (2020b) uses a similar expression but assumes an arbitrary constant temperature lapse rate and the factor T is replaced by the average temperature between the surface and the tropopause. We will not specify the exact expression we will use for the water vapor path, but simply note that both have the Clausius–Clapeyron scaling which depends on T more strongly than any prefactors, and assume that the optical depth scales with the water vapor path; therefore

$$\tau(T) \sim e^{-\frac{L_v}{R_v T}}, \tag{2}$$

where L_v is the latent heat of vaporization and R_v is the gas constant for water vapor. The approximate Clausius-Clapeyron scaling of water vapor optical depth near optically thick band centers (150 cm^{-1} and 1400 cm^{-1}) and over the optically thin window region (1000 cm^{-1}) are shown in Figure 1a for four line-by-line calculations with surface temperatures spanning from 275 K to 320 K. Consistent with prior work (Koll and Cronin 2018; Jeevanjee and Romps 2018), the $\tau(T)$ curve remains approximately invariant and increasing surface temperature only extends the curve to higher temperatures (Figure 1a, b).

Second, we approximate the Planck function using the Wien approximation,

$$B_{\tilde{\nu}}(T) \approx 2hc^2\tilde{\nu}^3 \exp\left(-\frac{hc\tilde{\nu}}{k_B T}\right), \tag{3}$$

where h is Planck's constant, k_B is Boltzmann's constant, and c is the speed of light. This approximation reproduces the high-wavenumber portion of the spectrum well and provides a reasonable representation at lower wavenumbers (Figure 1). Wien's formula was quickly superseded by Planck's law following its introduction around 1900. However, it remains useful for theoretical work in atmospheric radiation, where analytic tractability is often prioritized over exact accuracy. Relatively little work in atmospheric radiative transfer has explicitly exploited the Wien approximation, with Wordsworth et al. (2024) providing a recent example.

We may therefore define α and β as the fractional sensitivities of water-vapor optical depth and the Planck function, respectively, to temperature. From the Clausius–Clapeyron scaling (Eq. 2), the fractional increase of optical depth is

$$\alpha = \frac{\mathrm{d}\ln\tau}{\mathrm{d}T} \approx \frac{L_v}{R_v T^2}, \tag{4}$$

which has a typical magnitude of approximately 7% K^{-1} over the range of temperatures relevant to the Earth's atmosphere. The corresponding fractional increase of the Planck function under the Wien approximation (Eq. 3) is

$$\beta = \frac{\mathrm{d}\ln B_{\tilde{\nu}}}{\mathrm{d}T} \approx \frac{hc\,\tilde{\nu}}{k_B T^2}, \tag{5}$$

which exhibits the same inverse-squared temperature dependence but also varies with wavenumber. For a representative terrestrial infrared wavenumber of $\tilde{\nu} \approx 1000$ cm^{-1}, β is approximately 2% K^{-1}.

We have emphasized a structural similarity between water-vapor optical depth and Planck emission. This similarity is reflected in the near-linear relationships between $\ln\tau$ and $1/T$ (Figure 1b), and between $\ln B_{\tilde{\nu}}$ and $1/T$ (Figure 1d). The slope of the $\ln\tau$–$1/T$ relation is similar across the three wavenumbers and is approximately given by αT^2, whereas the slope of the $\ln B_{\tilde{\nu}}$–$1/T$ relation is approximately βT^2 and varies with wavenumber due to the $\tilde{\nu}$-dependence of β.

Dividing Eq. (5) by Eq. (4) yields

$$\frac{\mathrm{d}\ln B_{\tilde{\nu}}}{\mathrm{d}\ln\tau} = \frac{\beta}{\alpha} = \frac{R_v hc\tilde{\nu}}{L_v k_B}. \tag{6}$$

Because both α and β scale as T^{-2}, their ratio, which we define as γ, is independent of temperature, and is, therefore, constant at a given wavenumber $\tilde{\nu}$. As a result, the Planck function at wavenumber $\tilde{\nu}$ can be expressed as a power law in optical depth:

$$B_{\tilde{\nu}}(T(\tau)) \approx B_{\tilde{\nu}}(T_s)\left(\frac{\tau}{\tau_s}\right)^{\gamma}, \tag{7}$$

where the power-law exponent γ is

$$\gamma \equiv \frac{\beta}{\alpha} = \frac{R_v\, hc\,\tilde{\nu}}{L_v k_B} \tag{8}$$

and τ_s is the column optical depth or the surface optical depth.

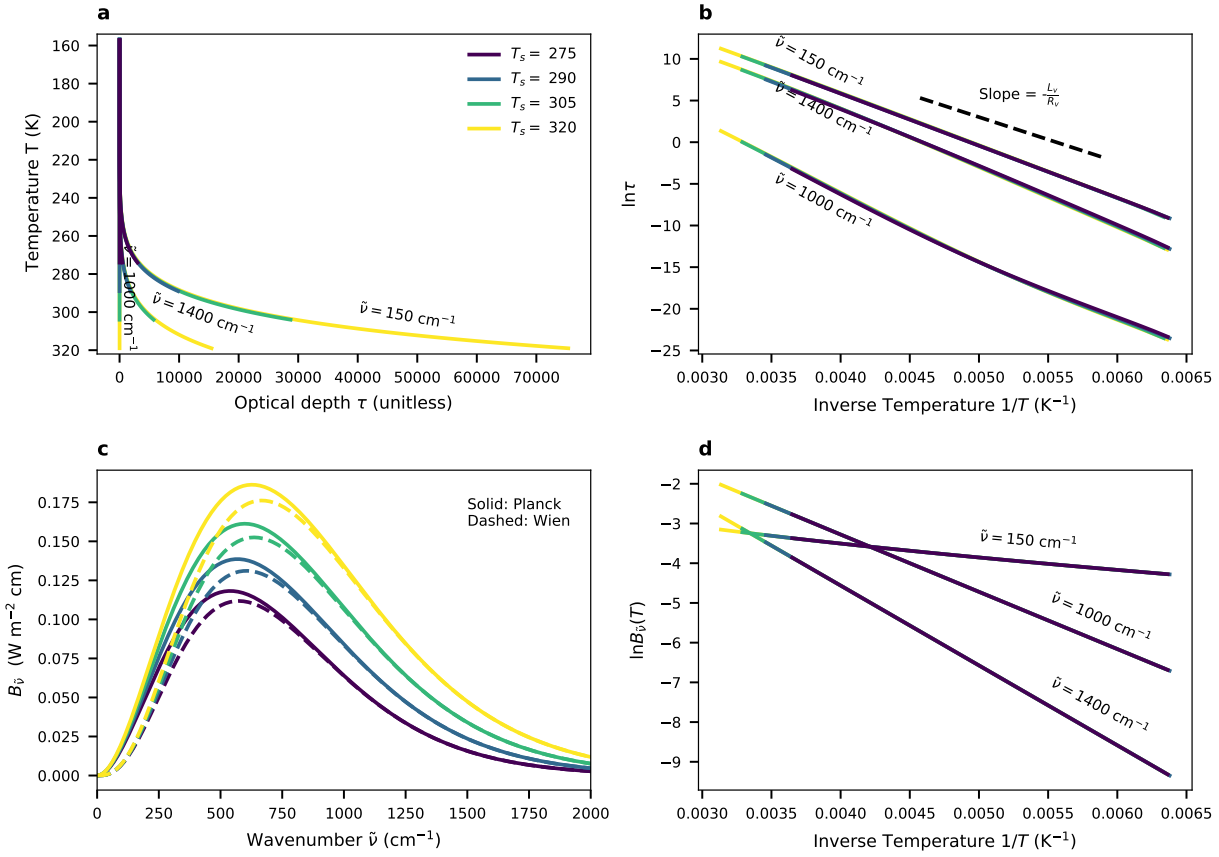

FIG. 1. Optical depth τ and Planck emission $B_{\tilde{\nu}}$ both exhibit an approximately exponential dependence on inverse temperature. (a) Optical depth profiles plotted against temperature show an approximately invariant structure, extending to higher temperatures as T_s increases. Wavenumbers of 150, 1000, and 1400 cm^{-1} are shown. (b) Corresponding near-linear relationships between $\ln\tau$ and $1/T$ for the same wavenumbers and surface temperatures as in (a). (c) The Planck function $B_{\tilde{\nu}}(T)$ (solid) compared with the Wien approximation (dashed) for the same T_s values. (d) Corresponding near-linear relationships between $\ln B_{\tilde{\nu}}(T)$ and $1/T$ for the same wavenumbers and surface temperatures as in (a).

b. Shared Boltzmann factor

Interestingly, the nondimensional parameter γ admits a simple physical interpretation. Using the relation $R_v = k_B/m_v$, where m_v is the molecular mass of water vapor (following from $R_v = R/M_v$ and $k_B = R/N_A$), and defining $l_v = L_v m_v$ as the latent heat released per H_2O molecule, Eq. (8) can be rewritten as

$$\gamma = \frac{h\nu}{l_v} = \frac{\text{photon energy}}{\text{latent heat per } H_2O \text{ molecule}}. \tag{9}$$

A characteristic window-region photon with $\tilde{\nu} = 1000\,\text{cm}^{-1}$ carries an energy of $h\nu = hc\tilde{\nu} \approx 2.0\times10^{-20}$ J, which is about one quarter of the latent heat release associated with condensation of a single water molecule ($l_v \approx 7.5\times10^{-20}$ J). Moving to a different $\tilde{\nu}$, a photon near the maximum of the rotational band ($\tilde{\nu} = 150\,\text{cm}^{-1}$) carries only about 4% of this latent energy l_v. Thus, γ is typically less than one for water vapor in Earth-like climate because a typical terrestrial infrared photon carries only a small fraction of the energy associated with condensation of a single H_2O molecule. The non-dimensional parameter γ incorporates two of water vapors roles in the atmosphere, that it is condensable therefore its distribution is strongly tied to temperature and that it absorbs and emits terrestrial radiation.

The shared exponential dependence on inverse temperature is instrumental to the power law and it is not a coincidence. The Wien approximation to the Planck function assumes that the photon occupation probability follows a Maxwell-Boltzmann distribution of the form $\exp(-E/k_BT)$, where the relevant energy scale E is the photon energy $h\nu$. The exponential temperature dependence of water-vapor optical depth follows from the Clausius–Clapeyron relation ($\sim\exp(-L_v/R_vT)$), which is usually derived from macroscopic thermodynamic laws rather than from a microscopic energy distribution. However, one may argue that the probability ratio of H_2O molecules in the

gas and liquid phases depends exponentially on the energy difference between these two states, $\exp(-\Delta E/k_B T)$, if both probabilities are assumed to follow Boltzmann statistics. When the vast majority of H_2O molecules remain in the liquid phase, the vapor number density and thus the vapor pressure would then scale with $\exp(-l_v/k_B T)$ (Bohren and Albrecht 2023; Lamb and Shaw 2016). In this sense, the shared exponential dependence on inverse temperature ultimately reflects the generality of the Boltzmann distribution in governing the statistics of microscopic states.

c. *Validation of the power law with line-by-line model*

We first test whether the power-law relation between the Planck function $B_{\tilde{\nu}}$ and optical depth τ, given by Eq. (7), holds. This relation relies on the assumption that τ scales linearly with the column-integrated water-vapor path, which is most appropriate for absorption at line centers. In contrast, the continuum arises from interactions between water-vapor molecules and exhibits an approximately quadratic dependence of τ on the water-vapor mixing ratio (Koll et al. 2023). Moreover, wavenumbers adjacent to multiple comparably strong lines receive contributions from the broadening of several lines, further complicating the dependence of τ on the water-vapor path. We thus first focus on spectrally isolated lines that clearly exceed neighboring lines in strength. For these cases, the $B_{\tilde{\nu}}$–τ power law holds remarkably well over a wide range of wavenumbers relevant for terrestrial radiation, as evidenced by the linear relationship in log–log space throughout the troposphere (Figure 2a). For the continuum, the log–log relationship exhibits minimal curvature (Figure A2) and a power law remains an accurate approximation overall. The results shown correspond to a representative surface temperature of 290 K and a vertically uniform relative humidity of 70%. As expected from theory, changes in relative humidity do not affect the slope in log–log space (i.e., the power-law exponent), but instead produce a vertical shift (see Appendix B and Figure A1).

We next test whether the theory for γ in Eq. (8) provides a good estimate of the power-law exponent across the thermal radiation spectrum (0–1600 cm^{-1}). The theory captures both the increase of the fitted exponent with wavenumber $\tilde{\nu}$ and its overall magnitude (Figure 2b), where spectral lines appear as sharp spikes (both upward and downward) in the fitted exponent and the continuum absorption manifests as a smooth background connecting these spikes. Agreement with theory is strongest for strongly absorbing wavenumbers, namely the band centers of the rotational band around 150 cm^{-1}, the vibration–rotation band around 1500 cm^{-1}, and many spectrally isolated lines at more weakly absorbing wavenumbers (upper tip of spikes in Figure 2b), including those in the window region. The continuum exhibits the strongest deviations from theory, consistent with its more complex dependence of optical

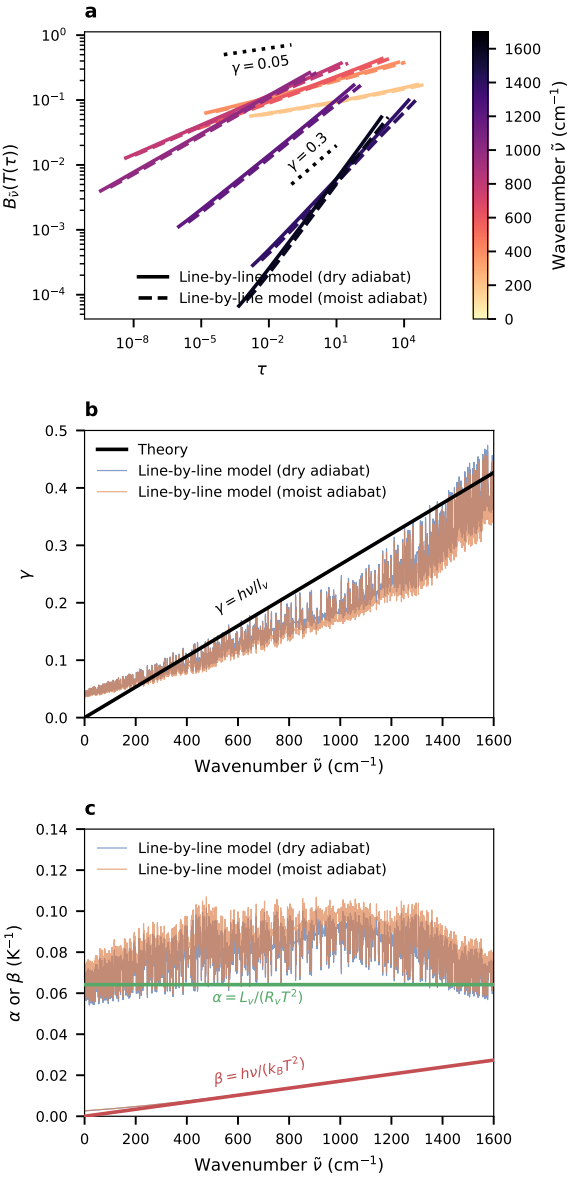

FIG. 2. Approximate power-law relation between the Planck function and optical depth. (a) For a surface temperature T_s = 290 K, the Planck function $B_{\tilde{\nu}}(T)$ is shown as a function of τ on logarithmic scales for the closeest spectrally isolated lines near the selected wavenumbers (200–1200 cm^{-1} in increments of 200 cm^{-1}). Isolated lines are identified based on τ_s exhibiting a distinct peak and all end up lie within 3 cm^{-1} of the target wavenumbers (see Figure 4d). Only the portion of the profile with temperature greater than 155 K is shown to exclude the stratosphere. Solid and dashed lines correspond to dry and moist adiabatic tropospheres, respectively. (b) Comparison of theoretical and fitted power-law exponents γ across the longwave spectrum. The fitted exponent is obtained from an ordinary least squares (OLS) regression of $\ln B_{\tilde{\nu}}$ against $\ln \tau$, with the slope giving γ. (c) Comparison of theoretical and fitted values of α and β. The fitted α is the slope obtained from an OLS regression of $\ln \tau$ against $-1/T$ for each wavenumber divided by the squared reference temperature of 290 K (Eq.4). The fitted β is obtained similarly from an OLS regression of $\ln B_{\tilde{\nu}}$ (Eq.5).

depth on water-vapor concentration. Using dry-adiabatic versus moist-adiabatic temperature profiles produces small differences in the inferred exponent with the dry adiabat being closer to the theory. Overall, the power-law approximation remains broadly valid across the thermal radiation spectrum.

Further insight is provided by examining the fractional sensitivities of optical depth R A N D the Planck function to temperature, namely α (Eq. 4) and β (Eq. 5). α shows the best agreement with the line-by-line estimate $\mathrm{d}\ln\tau/\mathrm{d}T$ at strongly absorbing wavenumbers and largely explains both the agreement and deviations of γ relative to the line-by-line results for wavenumbers above $200\,\mathrm{cm}^{-1}$ (Figure 2a). The deviation of β from the exact derivative $\mathrm{d}\ln B_{\tilde{\nu}}(T)/\mathrm{d}T$ arises solely from the use of the Wien approximation (Eq. 3), and is therefore confined to small wavenumbers (Figure 2c), where it largely accounts for the discrepancy between γ and the line-by-line calculations below $200\,\mathrm{cm}^{-1}$.

4. Approximate solutions to the Schwarzschild equations

The previous section shows that the power law (Eq. 7) provides a simple yet physically grounded approximation for $B_{\tilde{\nu}}(T(\tau))$. This allows the Schwarzschild equation in optical depth space (Eq. 1) to be written in the following form for the upward ($F^{\uparrow}_{\tilde{\nu}}$) and downward ($F^{\downarrow}_{\tilde{\nu}}$) fluxes, with corresponding boundary conditions:

$$\frac{\mathrm{d}F^{\uparrow}_{\tilde{\nu}}}{\mathrm{d}\tau} - F^{\uparrow}_{\tilde{\nu}} = -\pi B_{\tilde{\nu}}(T_s)\left(\frac{\tau}{\tau_s}\right)^{\gamma}, \quad F^{\uparrow}_{\tilde{\nu}}(\tau_s) = \pi B_{\tilde{\nu}}(T_s), \tag{10}$$

$$\frac{\mathrm{d}F^{\downarrow}_{\tilde{\nu}}}{\mathrm{d}\tau} + F^{\downarrow}_{\tilde{\nu}} = \pi B_{\tilde{\nu}}(T_s)\left(\frac{\tau}{\tau_s}\right)^{\gamma}, \quad F^{\downarrow}_{\tilde{\nu}}(0) = 0. \tag{11}$$

For the upward flux, the boundary condition is imposed at the surface ($\tau = \tau_s$), where the flux equals the surface Planck emission. For the downward flux, the boundary condition is imposed at the top of the atmosphere ($\tau = 0$), where there is zero incoming longwave radiation. The corresponding solutions to (10) and (11) are

$$F^{\uparrow}_{\tilde{\nu}}(\tau) = \pi B_{\tilde{\nu}}(T_s)\left[e^{-(\tau_s-\tau)} + \int_{\tau}^{\tau_s}\left(\frac{\tau'}{\tau_s}\right)^{\gamma} e^{-(\tau'-\tau)}\,\mathrm{d}\tau'\right], \tag{12}$$

$$F^{\downarrow}_{\tilde{\nu}}(\tau) = \pi B_{\tilde{\nu}}(T_s)\int_{0}^{\tau}\left(\frac{\tau'}{\tau_s}\right)^{\gamma} e^{-(\tau-\tau')}\,\mathrm{d}\tau', \tag{13}$$

where γ is defined in Eq (8). These solutions provide a good approximation to the line-by-line model results for both dry and moist adiabatic tropospheres, with the dry adiabatic lapse rate obtaining better agreements (Figure 3). Obtaining such approximate analytic solutions may facilitate further theoretical analysis and practical applications.

5. Spectral theory of the column-integrated cooling

a. Derivation

The column-integrated atmospheric longwave cooling at a given wavenumber is the net flux that goes out of the atmospheric column, achieved by computing $F^{\downarrow}_{\tilde{\nu}}(\tau_s) - F^{\uparrow}_{\tilde{\nu}}(\tau_s) + F^{\uparrow}_{\tilde{\nu}}(0)$ from (12) and (13):

$$Q_{\tilde{\nu}} = \underbrace{\pi B_{\tilde{\nu}}(T_s)\int_{0}^{\tau_s}\left(\frac{\tau}{\tau_s}\right)^{\gamma} e^{-\tau}\,\mathrm{d}\tau}_{\text{cooling to space } (Q_{\tilde{\nu},\mathrm{CTS}})} + \underbrace{\pi B_{\tilde{\nu}}(T_s)\int_{0}^{\tau_s}\left[\left(\frac{\tau}{\tau_s}\right)^{\gamma} - 1\right] e^{-(\tau_s-\tau)}\,\mathrm{d}\tau}_{\text{exchange with surface } (Q_{\tilde{\nu},\mathrm{EX}})}. \tag{14}$$

where the first term represents radiative exchange between all atmospheric layers and space, whose temperature is effectively 0 K, and is commonly referred to as the cooling-to-space term, while the second term represents radiative exchange between all atmospheric levels and the surface.

The cooling-to-space approximation (Green 1967; Jeevanjee and Fueglistaler 2020a) is a commonly invoked concept in atmospheric radiation. In its column-integrated form, this approximation states that the exchange-with-surface term is negligible, such that atmospheric cooling can be approximated by the cooling-to-space contribution alone,

$$Q_{\tilde{\nu}} \approx Q_{\tilde{\nu},\mathrm{CTS}}. \tag{15}$$

The accuracy of this approximation is analyzed in Section 7. Then we have

$$Q_{\tilde{\nu}} \approx \pi B_{\tilde{\nu}}(T_s)\,\Gamma(1+\gamma,\tau_s)\,\tau_s^{-\gamma}, \tag{16}$$

where $\Gamma(1+\gamma,\tau_s)$ denotes the lower incomplete gamma function, $\Gamma(1+\gamma,\tau_s) \equiv \int_0^{\tau_s}\tau^{\gamma}e^{-\tau}\,\mathrm{d}\tau$. The use of the incomplete Gamma function in atmospheric radiative transfer has precedents in Pierrehumbert (2010); Robinson and Catling (2012); Jeevanjee et al. (2021b); Tang and McColl (2025), as this form arises when a power-law relationship between the Planck emission $B_{\tilde{\nu}}(T)$ and optical depth τ is assumed. The main distinction here is that the exponent is determined by physical constants for each wavenumber (Eq. 8), whereas in prior work the power law is primarily a mathematical convenience and the exponent that may vary with τ and therefore does not constitute a strict power law.

b. Thick limit

We now examine the limiting behavior of Eq. (16). For very large column optical depth τ_s, corresponding to

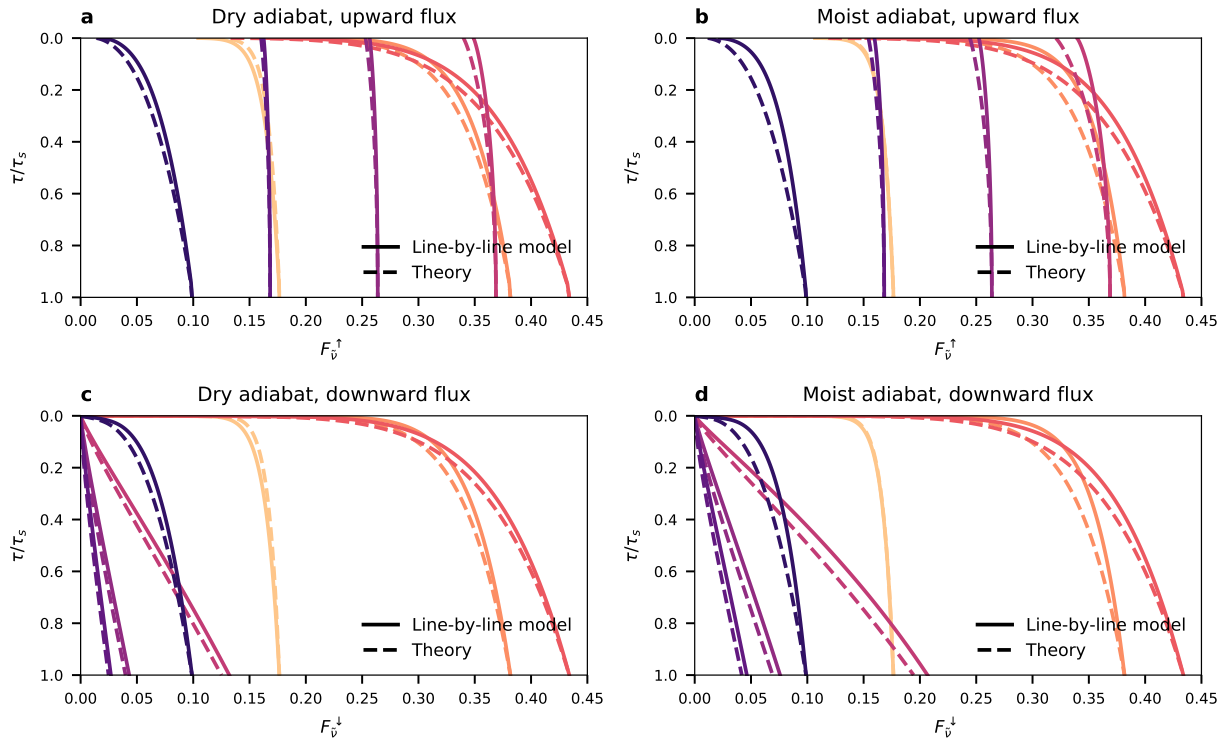

FIG. 3. Comparison of the approximate solutions (Eqs. 12 and 13) to the Schwartzchild equations with line-by-line model output for a surface temperature of 290 K. The atmospheric temperature profile follows either a dry adiabat (a, c) or a moist adiabat (b, d). Relative humidity is vertically uniform at 70%. An isothermal stratosphere at 150 K overlies the troposphere and contains no water vapor.

strongly absorbing water–vapor bands, the upper limit of the integral in Eq. (16) may be taken to infinity, since the integrand decays exponentially with τ. In this limit, the incomplete gamma function reduces to the ordinary gamma function, yielding

$$Q_{\tilde{\nu}} \approx \pi B_{\tilde{\nu}}(T_s)\,\Gamma(1+\gamma)\,\tau_s^{-\gamma}, \qquad \tau_s \gg 1. \tag{17}$$

Because $\Gamma(1+\gamma)$ deviates from unity by at most $\sim 10\%$ for $0 \le \gamma \le 1$, Eq. (17) admits an even simpler thick-limit form,

$$Q_{\tilde{\nu}} \approx \pi B_{\tilde{\nu}}(T_s)\,\tau_s^{-\gamma}, \qquad \tau_s \gg 1. \tag{18}$$

The key implication is that, for optically thick wavenumbers, both atmospheric cooling and outgoing longwave radiation (OLR) follow a power law with exponent $-\gamma$ (OLR is well approximated by $Q_{\tilde{\nu},\mathrm{CTS}}$ in this regime.) We make three remarks related to this.

(i) Weak sensitivity of cooling to RH. Because γ is small for wavenumbers relevant to thermal radiation, optically thick atmospheric cooling depends only weakly on the column optical depth τ_s. For example, taking $\gamma = 0.15$, representative of strong water–vapor cooling near $\tilde{\nu} \approx 600$ cm^{-1} (Figure 5a), a tenfold increase in τ_s reduces the cooling to about 70%, a thousandfold increase to roughly 30%, and even a millionfold increase only to 10%. Thus, very large changes in optical depth produce only modest changes in atmospheric cooling at fixed temperature.

This weak sensitivity has direct implications for relative humidity. If surface and atmospheric temperatures are held fixed, variations in relative humidity (RH) modify cooling through changes in τ_s, yielding

$$\frac{\partial \ln Q_{\tilde{\nu}}}{\partial \ln \mathrm{RH}} = -\gamma. \tag{19}$$

Hence, column-integrated cooling depends on RH through a power law with a small negative exponent. For typical free-tropospheric variations from 30% to 90% RH (a threefold increase in τ_s), this scaling implies a reduction in cooling of about 16% near $\tilde{\nu} \approx 600$ cm^{-1} and 34% near

$\tilde{\nu} \approx 1400\ \mathrm{cm}^{-1}$, at fixed surface temperature. This result is broadly consistent with the finding that tropospheric longwave cooling varies only weakly across climate zones with differing free-tropospheric RH (e.g., Figure 1 of Jeevanjee and Fueglistaler (2020b)), although previous arguments are regarding spectrally integrated, vertically resolved cooling.

(ii) The "$\tau = 1$" law. Equation (18) may also be interpreted as Planck emission originating from the level $\tau = 1$, once the power-law relation between the Planck function and optical depth in Eq. (7) is assumed:

$$Q_{\tilde{\nu}} \approx \pi B_{\tilde{\nu}}(T(1))\,. \tag{20}$$

This recovers the familiar "$\tau = 1$" law.

Retaining the $\Gamma(1+\gamma)$ factor instead of approximating it as unity, Eq. (17) may be rewritten as

$$Q_{\tilde{\nu}} \approx \pi B_{\tilde{\nu}}(T(\tau_{\mathrm{eff}}))\,, \qquad \tau_{\mathrm{eff}} \equiv \Gamma(1+\gamma)^{\frac{1}{\gamma}}. \tag{21}$$

The same formulation appears in Appendix B of (Jeevanjee et al. 2021b), where γ is defined more generally and estimated for CO_2 and water vapor. Using the present theory for γ, we obtain consistent values: at 600 cm^{-1}, $\tau_{\mathrm{eff}} \approx 0.63$ for $\gamma = 0.15$, and at 1500 cm^{-1}, $\tau_{\mathrm{eff}} \approx 0.74$ for $\gamma = 0.4$. These results confirm that the effective emission level remains of order unity for water vapor (Huang and Bani Shahabadi 2014; Jeevanjee and Romps 2018; Jeevanjee and Fueglistaler 2020b).

(iii) Simpson's law. Simpson's law states that in an atmosphere with constant relative humidity, the outgoing longwave radiation (OLR) at water-vapor-dominated wavenumbers does not change with surface warming (Simpson 1928; Ingram 2010; Jeevanjee et al. 2021a). Taking the derivative of the thick limit in Eq. (17) with respect to surface temperature T_s gives

$$\frac{\mathrm{d}Q_{\tilde{\nu}}}{\mathrm{d}T_s} \approx \frac{B_{\tilde{\nu}}(T_s)}{\tau_s^{\gamma}} \left(\frac{\mathrm{d}\ln B_{\tilde{\nu}}(T_s)}{\mathrm{d}T_s} - \gamma \frac{\mathrm{d}\ln \tau_s}{\mathrm{d}T_s} \right) = 0. \tag{22}$$

The last step follows from the definitions of α, β, and γ (Eqs. 4, 5, and 8). The power-law relation between the Planck function and optical depth thus automatically satisfies the invariance of OLR with respect to surface temperature changes and represents a simple analytical formulation of Simpson's law.

c. Thin limit

For wavenumbers where water vapor is not strongly absorbing and τ of any atmospheric level is much less than one, the exponential term ($e^{-\tau}$) in the integrand of Eq. (16) can be approximated as unity, yielding

$$Q_{\tilde{\nu}} \approx \pi B_{\tilde{\nu}}(T_s) \frac{\tau_s}{1+\gamma}, \qquad \tau_s \ll 1. \tag{23}$$

In this limit, atmospheric cooling scales linearly with the column optical depth.

d. Validation of cooling theory with line-by-line model

We test the lower incomplete Gamma-function approximation for column-integrated cooling $Q_{\tilde{\nu}}$ (Eq. 16) against line-by-line calculations. Because the exponent γ varies with wavenumber $\tilde{\nu}$ (Eq. 8), the dependence of $Q_{\tilde{\nu}}$ on column optical depth τ_s is likewise wavenumber dependent. We therefore evaluate the theory for water-vapor absorption lines near representative wavenumbers 200, 600, 1000, and 1400 cm^{-1} (Figure 4d), which together span much of the terrestrial thermal infrared spectrum and cover both the optically thin and thick regimes (Figure 4a,b).

In Eq. (16, the explicit dependence of $Q_{\tilde{\nu}}$ on surface temperature enters only through the prefactor $B_{\tilde{\nu}}(T_s)$. After normalization by $B_{\tilde{\nu}}(T_s)$, the theory predicts that results from different surface temperatures collapse onto a single curve when plotted against τ_s. This expectation is largely borne out by the line-by-line calculations: data spanning surface temperatures from 255 K to 320 K fall rather close to the theoretical curves. The normalized cooling increases linearly with τ_s in the optically thin regime, reaches a maximum for $\tau_s \sim O(1)$, and decreases as a power law with exponent $-\gamma$ in the optically thick limit (Figure 4a, b, and c).

The theory (Eq. 16) exhibits a high bias for $\tilde{\nu} \approx 200\ \mathrm{cm}^{-1}$ and smaller wavenumbers (not shown), but performs better at larger wavenumbers. This bias is likely due to the breakdown of the Wien approximation at low wavenumbers. As shown in Figure 2c, the Wien-based estimate of β is smaller than the Planck-based estimate, which propagates into an underestimate of the exponent γ. In the optically thick limit, where $Q_{\tilde{\nu}} \sim \tau_s^{-\gamma}$, this leads to a decay that is too slow with increasing τ_s. The actual decay is therefore steeper, resulting in an overestimate of $Q_{\tilde{\nu}}$ at small wavenumbers.

The line-by-line calculations also confirm the weak sensitivity of the results to relative humidity (RH). Data from experiments with RH of 30% and 70% form nearly indistinguishable curves (Figure 4a,b), consistent with the theory, in which RH enters only through its effect on the column optical depth τ_s.

6. Matched formulae for spectral cooling and OLR

Although the lower incomplete Gamma function is analytical and based on physical assumptions, it does not admit a closed-form expression and may therefore be less convenient for practical use. We thus provide simpler matched formulae that capture the asymptotic behavior of the incomplete gamma function, ensuring that the resulting approximation to the atmospheric cooling spectrum remains reasonably accurate while being easier to use.

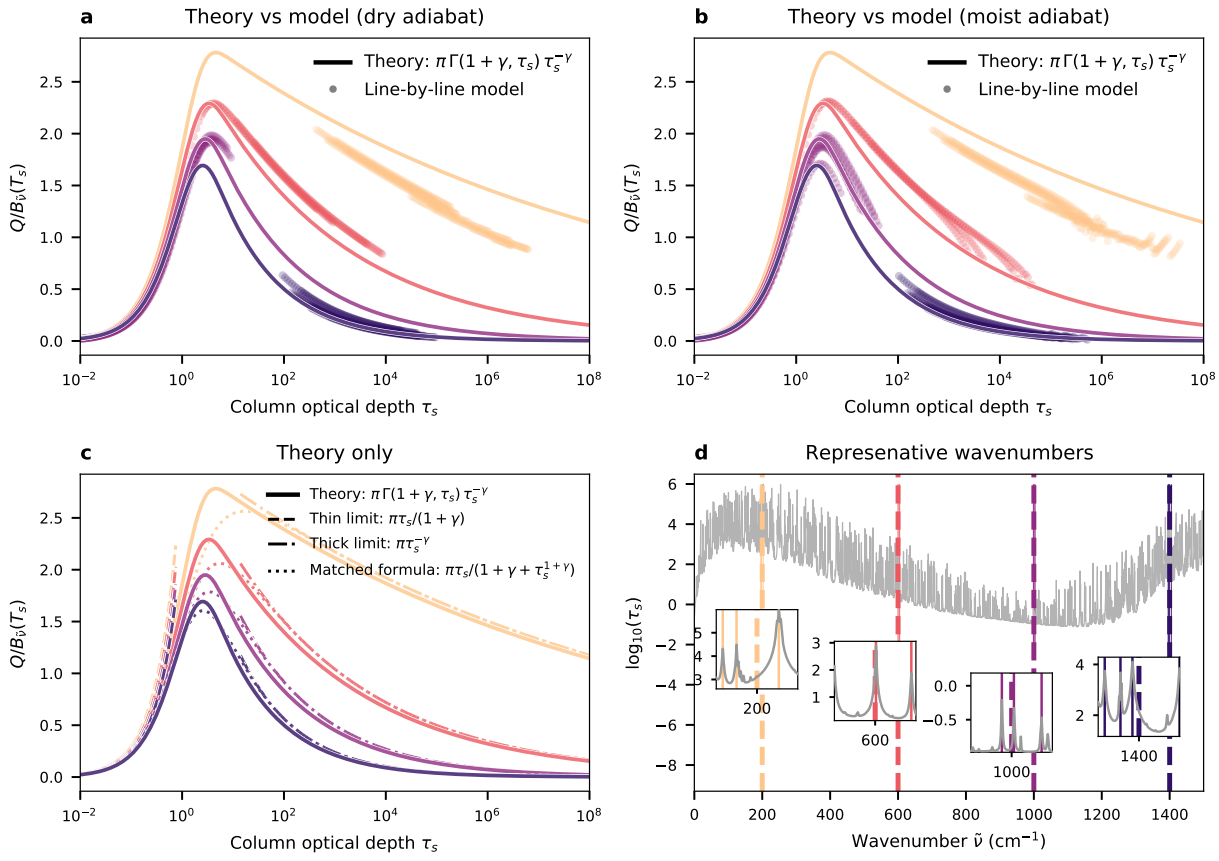

FIG. 4. The lower incomplete Gamma-function theory for atmospheric cooling, its limits, and comparison with line-by-line calculations. (a) Column-integrated atmospheric cooling, normalized by the surface Planck emission, $Q/B_\tilde{\nu}(T_s)$, as a function of column optical depth τ_s for representative wavenumbers 200, 600, 1000, and 1400 cm^{-1}. Solid curves show the lower incomplete Gamma-function prediction (Eq. 16). Dots indicate line-by-line radiative transfer calculations from PyRADS for water-vapor absorption lines within ± 5 cm^{-1} of each representative wavenumber. For each line, 130 data points are shown, corresponding to experiments with surface temperatures ranging from 255 K to 320 K, dry adiabatic lapse rates in the troposphere, and vertically uniform relative humidities of 30% and 70%. (b) Same as (a), but for experiments with moist adiabatic lapse rates in the troposphere. (c) The incomplete-Gamma-function theory, thin and thick limits (Eq. 24), and the formula matching both limits (Eq. 25) for the same wavenumbers. (d) Logarithm of column optical depth, $\log_{10}(\tau_s)$, as a function of wavenumber $\tilde{\nu}$ with zoomed-in insets for a reference state ($T_s = 290$ K, RH = 0.7) with a dry adiabatic lapse rate. Vertical colored lines mark the spectral lines shown in panels (a) and (b).

The incomplete-Gamma-function formulation of atmospheric cooling exhibits the following asymptotic behavior:

$$Q_\tilde{\nu} \sim \pi B_\tilde{\nu}(T_s) \begin{cases} \dfrac{\tau_s}{1+\gamma}, & \tau_s \to 0, \\ \tau_s^{-\gamma}, & \tau_s \to \infty, \end{cases} \tag{24}$$

where γ is the same exponent defined in Eq. (8). Matching the two limits in Eq. (24) yields the following expression:

$$Q_\tilde{\nu} \approx \pi B_\tilde{\nu}(T_s) \frac{\tau_s}{1+\gamma+\tau_s^{1+\gamma}}. \tag{25}$$

This expression transitions smoothly between the optically thin and thick regimes and provides a good approximation to the full lower incomplete Gamma-function expression (Eq. 16) across the range of γ relevant for the thermal spectrum (Figure 4c), while retaining the advantage of being fully algebraic.

Taking as input the surface temperature T_s and the optical depth of the column τ_s of each wavenumber $\tilde{\nu}$ we find that the incomplete Gamma function (Eq. 16) is in good agreement with the spectrum of column-integrated atmospheric cooling (Figure 5a). Moderate underestimates near 600 cm^{-1} exist for the moist adiabatic atmosphere. The matched formula in Eq. (25) also achieves a similar level of agreement over most of the spectrum.

We are able to treat the OLR spectrum similarly. The OLR at the top of the atmosphere is obtained by evaluating the upward flux (Eq. 12) at $\tau = 0$. This consists of the

sum of the atmospheric cooling-to-space term (first term in Eq. 14) and the attenuated surface emission. Replacing $Q_{\tilde{\nu},\mathrm{CTS}}$ with the incomplete Gamma-function expression (Eq. 16) yields

$$F^{\uparrow}_{\tilde{\nu}}(0) = \underbrace{\pi B_{\tilde{\nu}}(T_s)\,\Gamma(1+\gamma)\,\tau_s^{-\gamma}}_{\text{atmospheric emission } (=Q_{\tilde{\nu},\mathrm{CTS}} \approx Q_{\tilde{\nu}})} + \underbrace{\pi B_{\tilde{\nu}}(T_s)\,e^{-\tau_s}}_{\text{surface emission}}. \tag{26}$$

In the optically thick limit ($\tau_s \gg 1$), the surface contribution is exponentially suppressed, and the OLR approaches the atmospheric cooling-to-space term. In the optically thin limit ($\tau_s \ll 1$), atmospheric emission becomes negligible and the OLR approaches the surface Planck emission, $\pi B_{\tilde{\nu}}(T_s)$. The asymptotic behavior of $F^{\uparrow}_{\tilde{\nu}}(0)$ is therefore

$$F^{\uparrow}_{\tilde{\nu}}(0) \sim \begin{cases} \pi B_{\tilde{\nu}}(T_s), & \tau_s \to 0, \\ \pi B_{\tilde{\nu}}(T_s)\,\tau_s^{-\gamma}, & \tau_s \to \infty, \end{cases} \tag{27}$$

where γ is defined in Eq. (8).

A simple matched expression connecting these limits is

$$F^{\uparrow}_{\tilde{\nu}}(0) \approx \frac{\pi B_{\tilde{\nu}}(T_s)}{(1+\tau_s)^{\gamma}}, \tag{28}$$

which provides a compact analytic representation of the OLR spectrum as a function of optical depth and wavenumber. Similar forms have been proposed in Appendix C of Jeevanjee and Fueglistaler (2020a). The theory for OLR and the matched formula both reproduce the OLR spectrum for a reference temperature of 290 K with high fidelity (Figure 5b).

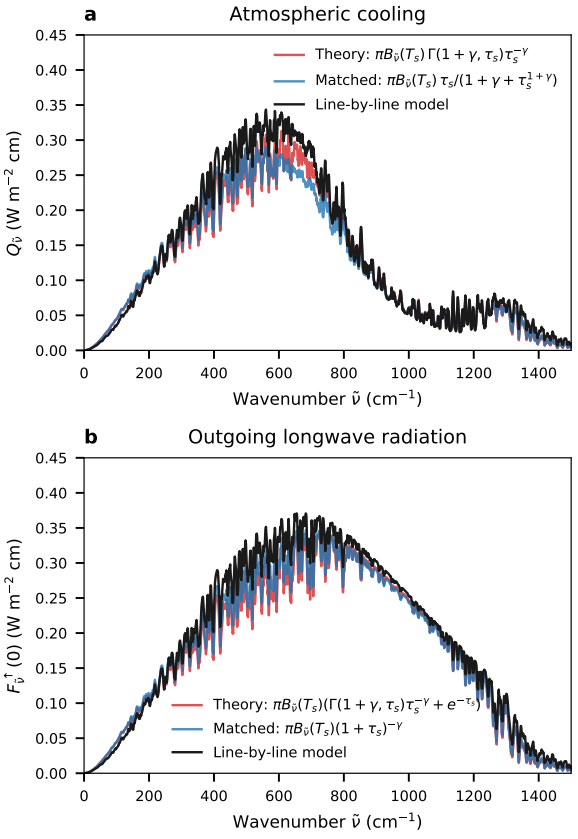

FIG. 5. Spectra of column-integrated cooling and outgoing longwave radiation compared with various approximations. Line-by-line results for a column with surface temperature 290 K, relative humidity 70%, and a dry adiabatic troposphere are shown in black in both panels. (a) Column-integrated cooling $Q_{\tilde{\nu}}$: the matched formula (Eq. 25) is shown in blue, and the theory based on the $B_{\tilde{\nu}}$–τ power-law relation (Eq. 16) is shown in red. (b) Outgoing longwave radiation: the matched formula (Eq. 28) is shown in blue, and the corresponding theory(Eq. 26) is shown in red. All spectra are smoothed using a rolling average over 5 cm^{-1}.

7. Accuracy of column-integrated cooling-to-space approximation

The theory of the column-integrated cooling spectrum in Section 5 is based on the cooling-to-space approximation, which neglects the exchange-with-surface term ($Q_{\tilde{\nu},\mathrm{EX}}$) in Eq. (14). The approximation is accurate across most of the spectrum, as illustrated in Fig. 6a, but here we formally estimate the accuracy of this approximation by estimating $Q_{\tilde{\nu},\mathrm{EX}}$.

Taylor expanding the Planck function $B_{\tilde{\nu}}(T(\tau))$ about τ_s and retaining terms up to linear order yields

$$Q_{\mathrm{EX}} \approx -\pi \left.\frac{\mathrm{d}B_{\tilde{\nu}}}{\mathrm{d}\tau}\right|_{\tau=\tau_s} \int_0^{\tau_s} (\tau_s - \tau)\, e^{-(\tau_s-\tau)}\,\mathrm{d}\tau \tag{29}$$

$$= -\pi\,\gamma\,\frac{B_{\tilde{\nu}}(T_s)}{\tau_s}\left[1-(\tau_s+1)e^{-\tau_s}\right], \tag{30}$$

where the second line follows from evaluating $\mathrm{d}B_{\tilde{\nu}}/\mathrm{d}\tau$ at τ_s using the Wien approximation and Clausius–Clapeyron scaling (Eqs. 4 and 5), together with $\gamma = \beta/\alpha$, giving

$$\left.\frac{\mathrm{d}B_{\tilde{\nu}}}{\mathrm{d}\tau}\right|_{\tau=\tau_s} = \gamma\,\frac{B_{\tilde{\nu}}(T_s)}{\tau_s}. \tag{31}$$

The relative error incurred by neglecting $Q_{\tilde{\nu},\mathrm{EX}}$ is

$$\eta \equiv -\frac{Q_{\tilde{\nu},\mathrm{EX}}}{Q_{\tilde{\nu},\mathrm{CTS}} + Q_{\tilde{\nu},\mathrm{EX}}}. \tag{32}$$

Substituting $Q_{\tilde{\nu},\mathrm{CTS}}$ with the matched expression Eq. (25) and $Q_{\tilde{\nu},\mathrm{EX}}$ with Eq. (30), η then depends only on τ_s for each $\tilde{\nu}$ (dashed lines in Fig. 6b).

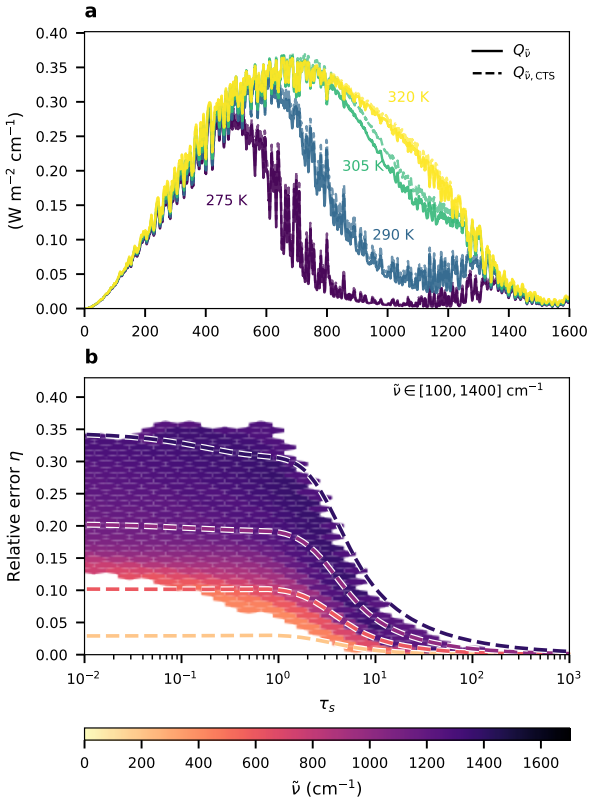

FIG. 6. The accuracy of the column-integrated cooling-to-space approximation is controlled by the smallness of γ. (a) Spectra of column-integrated atmospheric longwave cooling (solid) and the cooling-to-space term alone (dashed), computed from line-by-line radiative-transfer calculations for dry-adiabatic temperature profiles. See Eq. (14) for definition of the terms. Results are shown for surface temperatures ranging from 275 to 320 K in 15 K increments and vertically constant relative humidity of 70%. (b) Relative error η of the column-integrated cooling-to-space approximation. Hexagons show line-by-line results for surface temperatures ranging from 255 K to 320 K, wavenumbers from 100 to 1400 cm^{-1}, and RH values 0.3 and 0.7 binned in $(\tau_s, \tilde{\nu})$ space and colored by the median $\tilde{\nu}$. Only bins with more than 50 data points are shown (there is a total of 17 million data points). Superposed theoretical curves (Eq. 33) correspond to wavenumbers 200, 600, 1000 and 1400 cm^{-1}.

As $\tau_s \to \infty$, $\eta \to 0$, and the maximum error occurs in the optically thin limit $\tau_s \to 0$, for which

$$\lim_{\tau_s \to 0} \eta = \frac{\gamma(1+\gamma)}{2-\gamma(1+\gamma)} \tag{33}$$

The maximum η ranges from 0.02% for 150 cm^{-1} near the rotational band center to 34% for 1400 cm^{-1} near the right tail of Earth's Planck emission. At wavenumbers corresponding to the strongest cooling (approximately 400–800 cm^{-1}), the maximum η is modest, ranging from about 6% to 15%.

Eq. (33) suggests that the smaller γ is, the smaller the relative error induced by the column-integrated cooling-to-space approximation. This is qualitatively consistent with Jeevanjee and Fueglistaler (2020a), who argue that $\gamma \equiv \mathrm{d}\ln B_{\tilde{\nu}}/\mathrm{d}\ln\tau \ll 1$ is the criterion for the cooling-to-space approximation to hold near $\tau = 1$ when $\tau_s \gg 1$, whereas our argument concerns the column-integrated cooling-to-space approximation and is not limited to $\tau_s \gg 1$.

Combined with the interpretation of γ for a condensable gas as the ratio of photon energy to the latent heat released per molecule (Eq. 9), this implies that the cooling-to-space approximation is accurate in Earth-like climates but may not hold for RCE involving other condensable gases, depending on the latent heat of the gas and the wavenumbers with which it interacts.

8. Conclusions and future directions

We show that, over water–vapor–dominated wavenumbers, the Planck function $B_{\tilde{\nu}}$ varies approximately as a power law in optical depth τ (Eq. 7). The exponent γ admits a simple expression as fundamental physical constants and wavenumber (Eq. 8) and is given by the ratio of the energy of a terrestrial infrared photon to the latent heat released per water molecule (Eq. 9). This parameter γ encapsulates the dual physical role of water vapor as a condensable constituent of the atmosphere and as a radiatively active greenhouse gas. Because the latent heat of vaporization is large compared to the energy of a terrestrial infrared photon, γ remains small across the terrestrial infrared spectrum (Figure 2). The convenience that the Wien approximation to the Planck function might be useful in future work as well.

Using this Planck–optical-depth power law, we provide approximate solutions to the Schwartzchild equations for upward and downward longwave radiative fluxes (Eq. 12 and 13). We also derive an expression for the column-integrated cooling-to-space spectrum in terms of a lower incomplete Gamma function (Eq. 16). This expression unifies the optically thin and optically thick limits (Figure 4a-c) and reproduces the atmospheric cooling spectrum from line-by-line calculations (Figure 5).

The atmospheric cooling theory predicts limiting behaviors. In the optically thin limit ($\tau_s \to 0$), atmospheric cooling scales linearly with the column optical depth τ_s, while in the optically thick limit ($\tau_s \to \infty$) it follows a power law in τ_s with exponent $-\gamma$. Because γ is small, This scaling implies that atmospheric cooling decreases only weakly with increasing optical depth. This is equivalent to holding the surface temperature constant while increasing the relative humidity and consistent with that atmospheric cooling is insensitive to relative humidity. The same power law

also yields a simple analytical formulation of Simpson's law by automatically satisfying the invariance of OLR to surface warming (Eq. 22).

For ease of interpretation and future application, we develop a closed-form expression for atmospheric cooling (Eq. 25) that reproduce the optically thin and optically thick limits of the incomplete Gamma-function theory. Noting that the optically thin limit of outgoing longwave radiation (OLR) reduces to surface Planck emission, we also derive a corresponding matched expression for the OLR spectrum (Eq. 28). Comparisons with line-by-line radiative-transfer calculations demonstrate that these matched formulae accurately capture the spectral structure of both atmospheric cooling and OLR (Figure 5).

Lastly, we analyze the accuracy of the cooling-to-space approximation and find that the accuracy for the column-integrated cooing is ensured by the smallness of the nondimensional parameter γ. The smallness of γ traces back to the large latent heat of a water vapor molecule compared to the photon energy of thermal radiation.

This work can be extended in several directions. The present theory has been developed and tested for idealized column atmospheres with vertically uniform relative humidity and adiabatic temperature profiles. A natural next step is to evaluate its performance using observed atmospheric temperature and humidity profiles. Local and transient phenomena that deviate from column-mean behavior, such as temperature inversions, may become important and challenge the theory. Finally, applying similar reasoning to other condensable greenhouse gases or to non-Earth atmospheres may reveal whether analogous power-law structures more generally govern radiative cooling.

Acknowledgments. The author thanks Daniel Koll for making the PyRADS model publicly available (`https://github.com/danielkoll/PyRADS`), which makes use of HITRAN 2016 line lists (`http://hitran.org/`) and AER's MTCKD continuum model (`http://rtweb.aer.com/continuum_frame.html`). The author thanks Sean Cohen, Nadir Jeevanjee, Robert Pincus, and Adam Sobel for helpful feedback.

Data availability statement. All data used in the paper are model output of the PyRADS model which is freely available at `https://github.com/danielkoll/PyRADS`.

APPENDIX

Effect of relative humidity and continuum of absorption on the power law

The relative humidity (RH) does not affect the power-law scaling between $B_{\tilde{\nu}}$ and τ as long as it is vertically uniform. In that case, RH simply rescales the column optical depth τ_s, leading to a vertical shift in log–log space without changing the slope. This can be shown explicitly as follows.

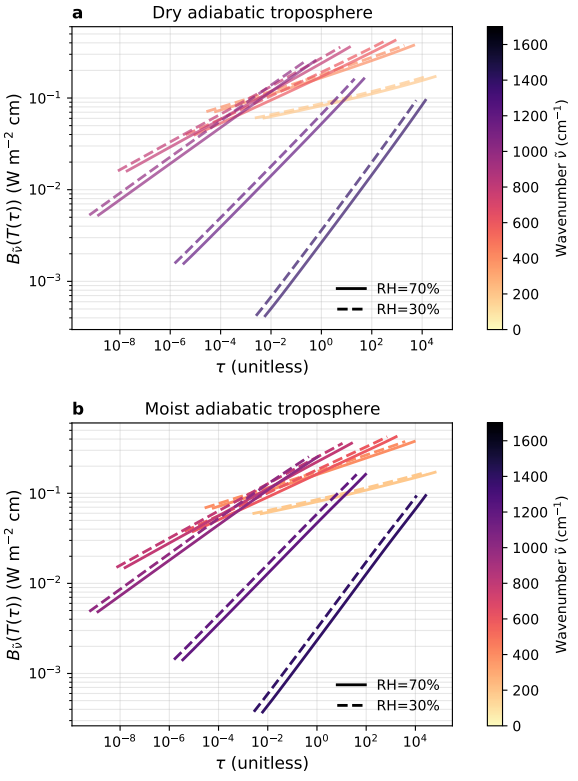

FIG. A1. Effect of relative humidity on the power-law scaling as a vertical shift in log–log space. (a) Dry adiabatic troposphere with surface temperature 290 K and vertically uniform relative humidity of 70% (solid) and 30% (dashed). (b) Same as (a), but for a moist adiabatic troposphere. Wavenumbers span 200–1600 cm^{-1} in increments of 200 cm^{-1}. The standalone lines, as in Figure 2a, are selected based on τ_s exhibiting a distinct peak of the target wavenumbers.

Assume two profiles with identical temperature structure but different constant relative humidities r_1 and r_2 and column optical depth $\tau_{s,1}$ and $\tau_{s,2}$. Since optical depth is proportional to the water-vapor path, we have

$$\frac{\tau_{s,1}}{\tau_{s,2}} = \frac{r_1}{r_2}. \tag{A1}$$

From the power-law relation in Eq. (7),

$$\ln B_{\tilde{\nu},1} = \gamma \ln \tau - \gamma \ln \tau_{s,1} \tag{A2}$$

$$\ln B_{\tilde{\nu},2} = \gamma \ln \tau - \gamma \ln \tau_{s,1} \tag{A3}$$

$$\tag{A4}$$

The two curves should then be offset by $\gamma \ln(r_1/r_2)$ in the log–log plot while the slope remains unchanged, as shown in Figure A1.

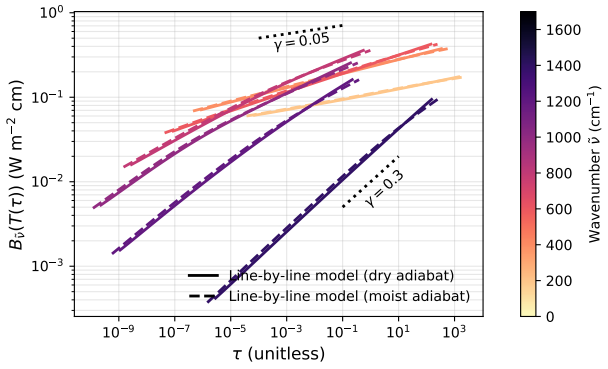

FIG. A2. Relationship between $B_{\tilde{\nu}}$ and τ, as in Figure 2a, but evaluated at wavenumbers exactly from 200 to 1600 cm^{-1} in increments of 200 cm^{-1}, rather than at the closest isolated lines.

References

Bohren, C., and B. Albrecht, 2023: *Atmospheric thermodynamics*. Oxford University Press.

Frierson, D. M., I. M. Held, and P. Zurita-Gotor, 2006: A gray-radiation aquaplanet moist gcm. part i: Static stability and eddy scale. *Journal of the atmospheric sciences*, **63 (10)**, 2548–2566.

Gordon, I. E., and Coauthors, 2022: The hitran2020 molecular spectroscopic database. *Journal of quantitative spectroscopy and radiative transfer*, **277**, 107 949.

Green, J., 1967: Division of radiative streams into internal transfer and cooling to space. *Quarterly Journal of the Royal Meteorological Society*, **93 (397)**, 371–372.

Hartmann, D. L., and K. Larson, 2002: An important constraint on tropical cloud-climate feedback. *Geophysical research letters*, **29 (20)**, 12–1.

Huang, Y., and M. Bani Shahabadi, 2014: Why logarithmic? a note on the dependence of radiative forcing on gas concentration. *Journal of Geophysical Research: Atmospheres*, **119 (24)**, 13–683.

Ingram, W., 2010: A very simple model for the water vapour feedback on climate change. *Quarterly Journal of the Royal Meteorological Society: A journal of the atmospheric sciences, applied meteorology and physical oceanography*, **136 (646)**, 30–40.

Jeevanjee, N., 2022: Three rules for the decrease of tropical convection with global warming. *Journal of Advances in Modeling Earth Systems*, **14 (11)**, e2022MS003 285.

Jeevanjee, N., and S. Fueglistaler, 2020a: On the cooling-to-space approximation. *Journal of the Atmospheric Sciences*, **77 (2)**, 465–478.

Jeevanjee, N., and S. Fueglistaler, 2020b: Simple spectral models for atmospheric radiative cooling. *Journal of the Atmospheric Sciences*, **77 (2)**, 479–497.

Jeevanjee, N., D. D. Koll, and N. Lutsko, 2021a: "simpson's law" and the spectral cancellation of climate feedbacks. *Geophysical Research Letters*, **48 (14)**, e2021GL093 699.

Jeevanjee, N., and D. M. Romps, 2018: Mean precipitation change from a deepening troposphere. *Proceedings of the National Academy of Sciences*, **115 (45)**, 11 465–11 470.

Jeevanjee, N., J. T. Seeley, D. Paynter, and S. Fueglistaler, 2021b: An analytical model for spatially varying clear-sky co 2 forcing. *Journal of Climate*, **34 (23)**, 9463–9480.

Koll, D. D., and T. W. Cronin, 2018: Earth's outgoing longwave radiation linear due to h2o greenhouse effect. *Proceedings of the National Academy of Sciences*, **115 (41)**, 10 293–10 298.

Koll, D. D., N. Jeevanjee, and N. J. Lutsko, 2023: An analytic model for the clear-sky longwave feedback. *Journal of the Atmospheric Sciences*, **80 (8)**, 1923–1951.

Lamb, D., and R. A. Shaw, 2016: Visualizing vapor pressure. *Bulletin of the American Meteorological Society*, **97 (8)**.

Manabe, S., and R. T. Wetherald, 1967: Thermal equilibrium of the atmosphere with a given distribution of relative humidity. *J. atmos. Sci*, **24 (3)**, 241–259.

Mlawer, E. J., V. H. Payne, J.-L. Moncet, J. S. Delamere, M. J. Alvarado, and D. C. Tobin, 2012: Development and recent evaluation of the mt_ckd model of continuum absorption. *Philosophical Transactions of the Royal Society A: Mathematical, Physical and Engineering Sciences*, **370 (1968)**, 2520–2556.

Pierrehumbert, R. T., 2010: *Principles of planetary climate*. Cambridge University Press.

Robinson, T. D., and D. C. Catling, 2012: An analytic radiative–convective model for planetary atmospheres. *The Astrophysical Journal*, **757 (1)**, 104.

Romps, D. M., 2014: An analytical model for tropical relative humidity. *Journal of Climate*, **27 (19)**, 7432–7449.

Seeley, J. T., N. Jeevanjee, and D. M. Romps, 2019: Fat or fitt: Are anvil clouds or the tropopause temperature invariant? *Geophysical Research Letters*, **46 (3)**, 1842–1850.

Simpson, S. G. C., 1928: *Some studies in terrestrial radiation*. Edward Stanford.

Tang, L. I., and K. A. McColl, 2025: Radiative–convective equilibrium over an idealized land surface with fixed soil moisture. *Journal of Climate*, **38 (22)**, 6639–6659.

Trenberth, K. E., J. T. Fasullo, and J. Kiehl, 2009: Earth's global energy budget. *Bulletin of the american meteorological society*, **90 (3)**, 311–324.

Wallace, J. M., and P. V. Hobbs, 2006: *Atmospheric science: an introductory survey*, Vol. 92. Elsevier.

Williams, A. I., and N. Jeevanjee, 2025: A robust constraint on the response of convective mass fluxes to warming. *Journal of Advances in Modeling Earth Systems*, **17 (4)**, e2024MS004 695.

Wordsworth, R., J. Seeley, and K. Shine, 2024: Fermi resonance and the quantum mechanical basis of global warming. *The Planetary Science Journal*, **5 (3)**, 67.